J Neurophysiol 91: 1457–1469, 2004.
First published December 10, 2003; 10.1152/jn.00989.2003.

TRANSLATIONAL PHYSIOLOGY

Cellular Effects of Deep Brain Stimulation: Model-Based Analysis of Activation and Inhibition

Cameron C. McIntyre,[1] Warren M. Grill,[2] David L. Sherman,[1] and Nitish V. Thakor[1]
[1]*Department of Biomedical Engineering, Johns Hopkins University School of Medicine, Baltimore, Maryland 21218; and* [2]*Department of Biomedical Engineering, Case Western Reserve University, Cleveland, Ohio 44195*

Submitted 14 October 2003; accepted in final form 2 December 2003

McIntyre, Cameron C., Warren M. Grill, David L. Sherman, and Nitish V. Thakor. Cellular effects of deep brain stimulation: model-based analysis of activation and inhibition. *J Neurophysiol* 91: 1457–1469, 2004. First published December 10, 2003; 10.1152/jn.00989.2003. Deep brain stimulation (DBS) is an effective therapy for medically refractory movement disorders. However, fundamental questions remain about the effects of DBS on neurons surrounding the electrode. Experimental studies have produced apparently contradictory results showing suppression of activity in the stimulated nucleus, but increased inputs to projection nuclei. We hypothesized that cell body firing does not accurately reflect the efferent output of neurons stimulated with high-frequency extracellular pulses, and that this decoupling of somatic and axonal activity explains the paradoxical experimental results. We studied stimulation using the combination of a finite-element model of the clinical DBS electrode and a multicompartment cable model of a thalamocortical (TC) relay neuron. Both the electric potentials generated by the electrode and a distribution of excitatory and inhibitory trans-synaptic inputs induced by stimulation of presynaptic terminals were applied to the TC relay neuron. The response of the neuron to DBS was primarily dependent on the position and orientation of the axon with respect to the electrode and the stimulation parameters. Stimulation subthreshold for direct activation of TC relay neurons caused suppression of intrinsic firing (tonic or burst) activity during the stimulus train mediated by activation of presynaptic terminals. Suprathreshold stimulation caused suppression of intrinsic firing in the soma, but generated efferent output at the stimulus frequency in the axon. This independence of firing in the cell body and axon resolves the apparently contradictory experimental results on the effects of DBS. In turn, the results of this study support the hypothesis of stimulation-induced modulation of pathological network activity as a therapeutic mechanism of DBS.

INTRODUCTION

Deep brain stimulation (DBS) has recently evolved from a highly experimental technique to a well-established therapy for the treatment of medically refractory movement disorders including dystonia, essential tremor, and Parkinson's disease (Gross and Lozano 2000). DBS results in clinical benefits analogous to those achieved by surgical lesions of the nucleus where the electrode is implanted. Three main targets have been identified that when ablated or stimulated result in beneficial clinical effects: the ventralis intermedius of the thalamus, the globus pallidus internus, and the subthalamic nucleus (Benabid et al. 1996; Gross and Lozano 2000; Obeso et al. 2001). Although the clinical benefits of DBS have been well documented, fundamental questions remain about the therapeutic mechanism(s) of action (Dostrovsky and Lozano 2002; Grill and McIntyre 2001; McIntyre and Thakor 2002; Montgomery and Baker 2000; Vitek 2002).

Because of the similarity in therapeutic outcomes achieved with DBS and lesions, it has been argued that high-frequency electrical stimulation (HFS) inactivates the structures being stimulated. Recordings made in the stimulated nucleus show inhibition and/or decreased activity during and after the stimulus train (Benazzouz et al. 1995, 2000; Boraud et al. 1996; Dostrovsky et al. 2000). However, recordings made in efferent nuclei of the stimulated nucleus indicate that the output of the stimulated nucleus is increased during DBS (Anderson et al. 2003; Hashimoto et al. 2003; Maurice et al. 2003; Windels et al. 2000, 2003). These results appear to be contradictory, with the former indicating that DBS inhibits the stimulated nucleus and the latter indicating that DBS excites the nucleus.

A significant obstacle in interpreting experimental results of DBS and developing a clear mechanism of action is the lack of quantitative understanding of the influence of HFS on the neural elements surrounding the electrode. Therefore we used detailed computer models of the stimulating electrode and surrounding neurons to determine the effects of stimulation in a controlled environment. Our approach combined a finite-element model of the clinical DBS electrode, a multi-compartment cable model of a thalamocortical (TC) relay neuron, and a distribution of excitatory and inhibitory synaptic inputs to the TC relay neuron. Each component of these models represents substantial improvement over our preliminary attempts to model the effects of thalamic stimulation where we used a point source electrode and ignored the effects of stimulation-induced trans-synaptic action (Grill and McIntyre 2001).

The first goal of this study was to determine whether HFS of the thalamus results in activation or inhibition of neurons surrounding the electrode. During extracellular stimulation, action potential initiation occurs in the axon (McIntyre and Grill 1999; Nowak and Bullier 1998a,b; Rattay 1999). Therefore we hypothesized that during HFS the activity recorded in the cell body of a neuron does not accurately reflect the efferent output, and a neuron could simultaneously exhibit suppression of activity in the soma and excitation of the axon (Grill and

Address for reprint requests and other correspondence: C. C. McIntyre, Cleveland Clinic Foundation, Department of Biomedical Engineering, 9500 Euclid Avenue, ND20, Cleveland, OH 44195 (E-mail: mcintyre@bme.ri.ccf.org).

The costs of publication of this article were defrayed in part by the payment of page charges. The article must therefore be hereby marked "*advertisement*" in accordance with 18 U.S.C. Section 1734 solely to indicate this fact.

McIntyre 2001; McIntyre and Grill 2002). This hypothesis, if supported, resolves the apparently conflicting experimental results indicating that DBS both inhibits and excites the stimulated nucleus.

The second goal of this study was to determine the spatial extent of activation and/or inhibition of neurons surrounding the electrode generated with therapeutic stimulation parameters. Presently, the stimulus parameters used in clinical DBS (monopolar or bipolar stimulation; 120 to 180 Hz stimulus frequency; 0.06 to 0.2 ms pulse duration; 1 to 5 V stimulus amplitude) are derived by trial and error (O'Suilleabhain et al. 2003; Volkmann et al. 2002). Understanding the impact of parameter variation on the effects DBS represents an important step in developing rational methods for system design and tuning (Benabid et al. 2000).

METHODS

This study combined a finite-element model of the electric field generated by a DBS electrode and a multi-compartment cable model of a thalamocortical (TC) relay neuron to examine the cellular effects of high-frequency extracellular stimulation. The electric field model included a representation of the DBS lead surrounded by homogeneous brain tissue and was used to determine the extracellular potential distribution generated by DBS. The neuron model included explicit geometrical representations of the dendritic arbor, cell body, and myelinated axon and nonlinear membrane dynamics representing the ion channel distributions in each section of the neuron. The resulting integrated model allowed the study of the neuronal output as a function of extracellular stimulation with DBS electrodes.

DBS electrode model

We developed an axisymmetric finite-element model of the Medtronic 3387 DBS lead (Medtronic, Minneapolis, MN) positioned in a homogeneous isotropic volume conductor to solve for the potential distribution generated in the tissue medium (Fig. 1). The model was implemented using 4-node quadrilateral elements in a commercially available software package (ANSYS 5.7, ANSYS, Houston, PA). The voltages (V) at the nodes of the finite-element mesh were calculated using a frontal solution method of the Laplace equation

$$\nabla \times \sigma \nabla V = 0$$

where $\sigma = 350\ \Omega\ \mathrm{cm}^{-1}$ (Sances and Larson 1975) was the electrical conductivity of the tissue medium (Fig. 1). The model consisted of 15,782 nodes. Along the surface of the electrode contact the separation between the nodes of the finite-element mesh was 25 μm, and in the tissue within 5 mm surrounding the electrode the spacing between nodes was <50 μm. The tissue box surrounding the electrode was 50×50 mm with the outer boundary set to 0 V, and the electrode contact set to the stimulus voltage. Doubling the density of the mesh or doubling the distance of the boundary from the electrode (i.e., the size of the tissue box) generated a potential distribution that differed by $<2\%$ when compared with the default model.

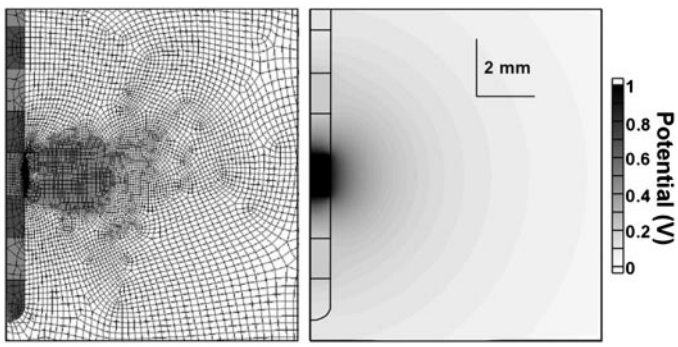

FIG. 1. Finite-element model of the electric potential distribution generated by a deep brain stimulation (DBS) electrode. An axisymmetric model of the Medtronic 3387 DBS electrode was constructed (dark gray: electrode insulation; gray: electrode contact; white: tissue medium) using a nonuniform mesh density to increase accuracy near the electrode contact (*left*). *Right*: potential distribution generated in the tissue medium by a 1-V stimulus with the DBS electrode.

The extracellular potential (V_e) generated by the DBS electrode model was applied to the TC relay neuron model (see description below) during time periods when the stimulus pulse was on to determine the influence of the electric field on neural excitation. Each compartment of the neuron model (n) was assigned a $V_e[n]$ that corresponded to the compartment position (X[n], Y[n], Z[n]) relative to the electrode. These extracellular potentials were determined from the DBS electrode model by defining the radial distance from electrode to the neuron compartment as $R[n] = (X[n]^2 + Z[n]^2)^{1/2}$ and Y[n] as the vertical position of the neural compartment relative to the center of the electrode contact. The position of each of the neural compartments (R[n], Y[n]) did not necessarily correspond to the position of a node in the finite-element mesh. Therefore a 4-point 2-dimensional linear interpolation algorithm was used to calculate $V_e[n]$, and the mesh density in the tissue medium was such that cubic and linear interpolation of the potential differed by $<1\%$ (McIntyre and Grill 2001). During each time step of the simulation the V_e for each compartment was set either to zero when no stimulus pulse was being applied or to the potentials generated by the DBS electrode when a stimulus pulse was being applied (McNeal 1976).

Thalamocortical relay neuron model

The DBS electrode model was coupled to a three-dimensional (3-D) multi-compartment cable model of a TC relay neuron. The model consisted of a dendritic tree, cell body, and myelinated axon with a geometry obtained from a 3-D reconstruction of a filled cell (Destexhe et al. 1998) (Fig. 2, Table 1). The membrane of the TC model consisted of the membrane capacitance (1 μF/cm^2: cell body and dendrites; 2 μF/cm^2: myelinated axon), in parallel with a complement of linear leakage and nonlinear calcium, potassium, and sodium conductances distributed in the different sections of the neuron (Fig. 2). The compartments were connected together with linear resistors based on the geometry of the connecting compartments and the intracellular resistivity (300 Ω cm^{-1}: cell body and dendrites; 70 Ω cm^{-1}: myelinated axon).

The membrane models of the cell body and dendritic tree of the TC relay neuron were based on the results of previous modeling and experimental studies (Destexhe et al. 1998; Huguenard and McCormick 1992; McCormick and Huguenard 1992; Williams and Stuart 2000). The cell body and dendritic compartments included the parallel combination of nonlinear fast Na^+, delayed rectifier K^+, slow K^+, T-type Ca^{2+}, and hyperpolarization-activated cation conductances, Na^+ and K^+ linear leakage conductances, and the membrane capacitance (Fig. 2; Table 2; see APPENDIX). The initial segment compartments included the parallel combination of nonlinear fast Na^+, delayed rectifier K^+, and slow K^+ conductances, a linear leakage conductance, and the membrane capacitance (Fig. 2; Table 2; APPENDIX).

The myelinated axon (diameter: 2 μm) used a concentric double-cable structure with explicit representations of the nodes of Ranvier, myelin attachment segment (MYSA), paranode main segment (FLUT), and internode segment (STIN) regions of the fiber (Fig. 2; Table 3; APPENDIX) (McIntyre et al. 2002). Between each node there were 2 MYSA compartments, 2 FLUT compartments, and 3 STIN compartments. The nodes included the parallel combination of nonlinear fast Na^+, persistent Na^+, and slow K^+ conductances, a linear leakage conductance, and the membrane capacitance. The paranodal and internodal compartments included 2 concentric layers, each in-

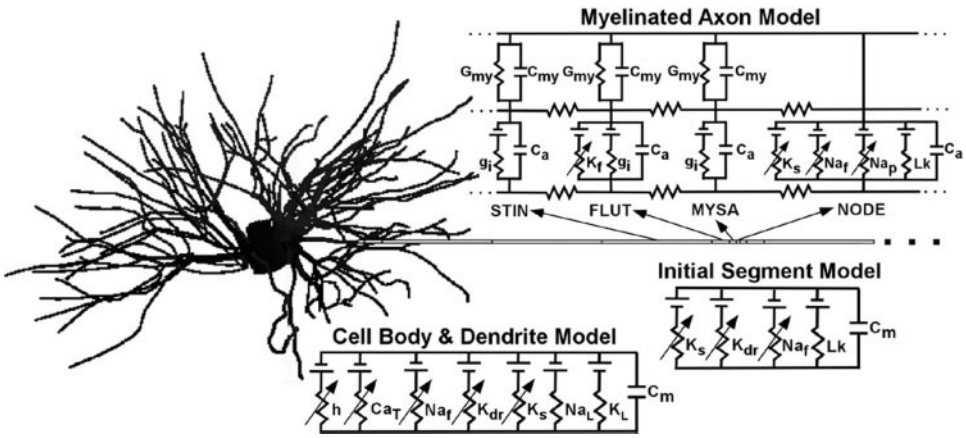

FIG. 2. Cable model of a thalamocortical relay neuron. Model consisted of a 3-D branching dendritic tree, multi-compartment soma and initial segment, and a myelinated axon with explicit representation of the myelin and underlying axolemma. Distribution and electrical properties of the ion channels in the dendrites, cell body, and axon were derived from voltage- and current-clamp measurements on mammalian neurons. Intracellular resistors, determined by the dimensions of the adjoining compartments, connected the different elements of the model together.

cluding a linear conductance in parallel with the membrane capacitance, to represent the myelin sheath and underlying axolemma. The FLUT sections of the model also contained a fast K^+ conductance in the axolemma.

Synaptic input models

Previous work has shown that the threshold for extracellular stimulation of axonal terminals projecting to the region around the electrode is lower than the threshold for direct activation of local cells (Baldissera et al. 1972; Dostrovsky et al. 2000; Gustafsson and Jankowska 1976; Jankowska et al. 1975; McIntyre and Grill 2002). We modeled the trans-synaptic effect of extracellular stimulation on local cells by applying either excitatory or inhibitory synaptic conductances to each of the dendritic and somatic compartments of the TC neuron. The distribution of inhibitory and excitatory synapses was based on electron microscopic reconstructions of the glutamateric and GABAergic terminals on TC neurons (Sato et al. 1997). Each compartment was designated as either proximal (0–44 μm), medial (45–90 μm), or distal (>90 μm) relative to the cell body. The compartments within each group (proximal, medial, distal) were randomly assigned as either excitatory or inhibitory with proportions based on the experimental distribution of synaptic inputs: proximal: 30% excitatory, 70% inhibitory; medial: 50% excitatory, 50% inhibitory; distal: 70% excitatory, 30% inhibitory (Sato et al. 1997) (Fig. 6*A*).

Four types of synaptic conductances were used: AMPA, NMDA, GABAa, and GABAb. The time course and amplitude of the synaptic conductances were modeled with first-order kinetics of the binding of transmitter to postsynaptic receptors (Destexhe et al. 1994a,b)

$$dR/dt = \alpha C(1 - R) - \beta R$$

where C is the concentration of neurotransmitter in the synaptic cleft, α and β are the forward and backward rate constants, and R represents the fraction of open channels on the postsynaptic membrane. When the receptor is activated, C instantaneously changes from zero to 1 mM and remains there for 1 ms (AMPA, NMDA, GABAa) or 84 ms (GABAb). The postsynaptic current in the compartments receiving inhibitory stimulation-induced trans-synaptic inputs is given by

$$I_{GABAa} = g_{GABAa}R_{GABAa}(V_m - E_{GABAa})$$

$$I_{GABAb} = g_{GABAb}R_{GABAb}(V_m - E_{GABAb})$$

and in the compartments receiving excitatory stimulation-induced trans-synaptic inputs by

$$I_{AMPA} = g_{AMPA}R_{AMPA}(V_m - E_{AMPA})$$

$$I_{NMDA} = g_{NMDA}B(V_m)R_{NMDA}(V_m - E_{NMDA})$$

$$B(V_m) = 1/(1 + 0.28e^{(-0.62V_m)})$$

where V_m is the postsynaptic membrane potential, g is the maximal conductance of each synapse, B is the Mg^{2+} block of the NMDA

TABLE 1. *Model geometric parameters*

Cell body	
Soma compartments	3
Soma surface area	3,171 μm^2
Initial segment compartments	3
Initial segment surface area	173 μm^2
Dendrites	
Dendritic compartments	251
Primary dendrites	11
Dendritic surface area	21,356 μm^2
Myelinated axon	
Fiber diameter	2 μm
Number of myelin lamella	30
Node length	1 μm
Node diameter	1.4 μm
MYSA length	3 μm
MYSA diameter	1.4 μm
MYSA periaxonal space width	0.002 μm
FLUT length	10 μm
FLUT diameter	1.6 μm
FLUT periaxonal space width	0.004 μm
STIN length	57.7 μm
STIN diameter	1.6 μm
STIN periaxonal space width	0.004 μm

TABLE 2. *Cell body and dendrite electrical parameters*

Na^+ Nernst potential (E_{Na})	45 mV
K^+ Nernst potential (E_K)	−95 mV
Leakage reversal potential (E_{Lk})	−70 mV
Soma and dendrite parameters	
Max. T-type Ca^{2+} permeability (P_{CaT})	0.0001 cm/s
Max. fast Na^+ conductance (g_{Naf})	0.03 S/cm^2
Max. delayed rectifier K^+ conductance (g_{Kdr})	0.003 S/cm^2
Max. slow K^+ conductance (g_{KS})	0.0007 S/cm^2
Max. I_h conductance (g_h)	0.0005 S/cm^2
Na^+ leakage conductance (g_{NaL})	0.0000095 S/cm^2
K^+ leakage conductance (g_{KL})	0.00005 S/cm^2
Initial segment parameters	
Max. fast Na^+ conductance (g_{Naf})	0.3 S/cm^2
Max. delayed rectifier K^+ conductance (g_{Kdr})	0.03 S/cm^2
Max. slow K^+ conductance (g_{KS})	0.007 S/cm^2
Leakage conductance (g_{Lk})	0.00005 S/cm^2

TABLE 3. *Axon electrical parameters*

Axon internode parameters	
Myelin conductance (g_{my})	0.001 S/cm^2
Myelin capacitance (c_{my})	0.1 μF/cm^2
MYSA leakage conductance (g_i)	0.0001 S/cm^2
FLUT leakage conductance (g_i)	0.0001 S/cm^2
FLUT fast K^+ conductance (g_{Kf})	0.02 S/cm^2
STIN leakage conductance (g_i)	0.0001 S/cm^2
Axon node parameters	
Max. fast Na^+ conductance (g_{Naf})	3.0 S/cm^2
Max. persistent Na^+ conductance (g_{Nap})	0.05 S/cm^2
Max. slow K^+ conductance (g_{Ks})	0.07 S/cm^2
Leakage conductance (g_{Lk})	0.005 S/cm^2

conductances, and E is the synaptic reversal potential. The parameters describing the synaptic currents are listed in Table 4 and were fit to experimental recordings using a simplex algorithm (Destexhe et al. 1994a,b).

To simulate the effect of a large numbers of synaptic inputs activated during DBS, each synapse on the entire soma–dendritic architecture was initiated simultaneously in response to each applied stimulus pulse. All simulations that incorporated stimulation-induced trans-synaptic effects assumed that the stimulation was always suprathreshold for activation of the presynaptic axon terminals. The threshold voltage to activate a presynaptic axon terminating in a synaptic bouton was approximately half of the threshold voltage to activate the postsynaptic neuron (data not shown). The default values of the excitatory synaptic conductances were set such that the membrane depolarization generated by the simultaneous activation of all the AMPA and NMDA conductances was 3 times the threshold for action potential initiation when the conductances were activated from rest with no other concomitant influences. The default values of the GABAa and GABAb conductances generated a peak hyperpolarization of 15 mV of when activated from rest with no other concomitant influences.

RESULTS

Model-based analysis of the cellular effects of DBS revealed both excitatory and inhibitory effects on the neural elements near the electrode. The response of TC relay neurons to DBS was dependent on 3 main factors: the positioning of the neuron with respect to the electrode, the stimulation parameters (pulse amplitude, pulse duration, frequency), and the stimulation-induced trans-synaptic influences. Clinically effective stimulation parameters (−3 V, 0.1 ms pulses at 150 Hz) resulted in either efferent output at the stimulus frequency or a suppression of intrinsic firing by stimulation-induced trans-synaptic inputs. In neurons exhibiting efferent activation, the cell body was suppressed, whereas the axon followed one to one with the stimulus frequency and thus the activity recorded in the cell body of neurons suprathreshold for activation was not a faithful representation of axonal output during HFS.

Electrophysiological properties of the thalamocortical relay neuron model

The firing properties of the model were compared with the electrophysiological properties of thalamic neurons measured in vitro (Emri et al. 2000; Jahnsen and Llinas 1984; Pape and McCormick 1995) (Fig. 3). The neuron model had a resting membrane potential of −70 mV, and an input resistance of 54 MΩ as recorded in the soma. The model reproduced experimentally recorded membrane potential–dependent firing properties. A constant current stimulus injected in the soma elicited a passive response, burst response, or tonic firing depending on the membrane potential of the soma (Fig. 3*A*) (Jahnsen and Llinas 1984). The model exhibited rebound excitation from a hyperpolarizing stimulus that corresponded to experimental data. As the amplitude of the hyperpolarization was increased the degree of inward rectification increased and after release from the hyperpolarization bursts of action potentials were generated (Fig. 3*B*) (Pape and McCormick 1995). Constant current injection in the soma generated a firing frequency that matched well with experimental measurements (Fig. 3*C*) (Pape and McCormick 1995). In addition, decreasing the Na^+ leakage conductance, increasing the T-type Ca^{2+} conductance, and shifting the voltage dependency of I_h resulted in a model that exhibited an intrinsic delta oscillation that corresponded to experimental bursting patterns (Fig. 3*D*) (Emri et al. 2000). Thus the model was able to replicate a wide range of experimentally documented excitation properties of thalamic neurons.

Extracellular stimulation of thalamic neurons: effects on resting neurons

The potentials generated by the DBS electrode model were applied to the TC relay neuron to determine the effects of extracellular stimulation. The application of extracellular electric fields results in regions of both depolarization and hyperpolarization in the same neuron (McIntyre and Grill 1999; Rattay 1999). The spatial distribution of polarization is dependent on the second derivative of extracellular potential along each neuronal process, and thus the position of the neuron with respect to the electrode affects its polarization. Figure 4 shows an example of the response of the TC relay neuron with its cell body located 1.5 mm from the geometric center of the stimulating contact and its axon oriented parallel to the electrode shaft. The cell body and dendritic arbor exhibited a complex pattern of depolarization and hyperpolarzation during the stimulus pulse, but the axonal elements near the cell body were all depolarized by the stimulus (Fig. 4). In this example, and in every neuron orientation we examined, action potential initiation took place in the axon.

Clinically effective DBS uses continuous trains of short-duration cathodic stimuli at frequencies above 100 Hz (Benabid et al. 1996). Therefore we examined the response of the TC relay neuron to HFS. Intracellular stimulation applied in the cell body generated action potentials in the cell body that were transmitted down the axon in a 1:1 ratio with the stimulus frequency (Fig. 5). However, extracellular DBS of the neuron in Fig. 4 resulted in independent firing of the cell body and axon at high stimulation frequencies. As with intracellular stimulation, the axon responded one to one with the stimulus frequency, but the cell body was unable to follow high stimulus frequencies (Fig. 5). This decoupling of somatic firing and

TABLE 4. *Synaptic input parameters*

	g, nS	α, mM^{-1} ms^{-1}	β, ms^{-1}	E, mV
AMPA	0.5	1.1	0.19	0
NMDA	2	0.072	0.0066	0
GABAa	5	0.53	0.184	−85
GABAb	0.2	0.016	0.0017	−95

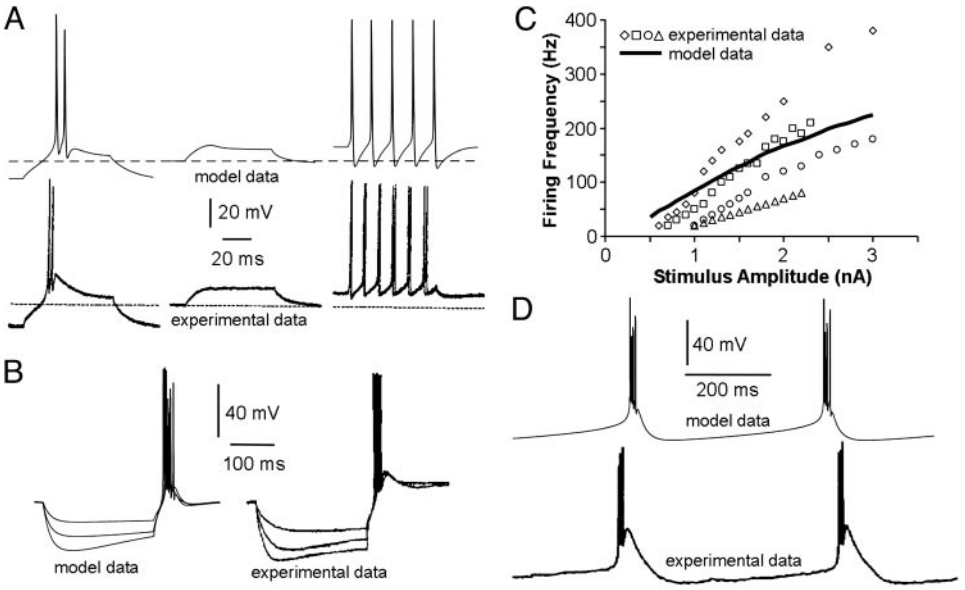

FIG. 3. Excitability properties of thalamic neurons. Model exhibited excitation properties that matched well with experimental records including membrane potential dependent firing properties [*A*: experimental comparison from Jahnsen and Llinas (1984)], rebound excitation [*B*: experimental comparison from Pape and McCormick (1995)], and firing frequency as a function of stimulus amplitude [*C*: experimental comparison from Pape and McCormick(1995)]. *D*: intrinsic bursting was obtained by reducing the somatic and dendritic Na^+ leakage conductance (g_{NaL} = 0 S/cm^2), increasing the T-type Ca^{2+} permeability (P_{CaT} = 0.0002 cm/s), and shifting the voltage dependency of I_h (+5 mV shift) [experimental comparison from Emri et al. (2000)].

axonal firing was achieved without stimulation-induced trans-synaptic inputs.

In general, presynaptic axon terminals have lower thresholds for activation than local cells with DBS stimulation parameters (Baldissera et al. 1972; Dostrovsky et al. 2000; Gustafsson and Jankowska 1976; Jankowska et al. 1975; McIntyre and Grill 2002). Therefore a large number of synaptic inputs impinging on local cells will be activated by DBS, and can thus alter the firing of local cells during DBS. We determined the effect of stimulation-induced trans-synaptic activity on the TC relay neuron with a distribution of AMPA, NMDA, GABAa, and GABAb synaptic conductances on the dendrites and cell body (see METHODS). Figure 6 shows the influence of stimulation-induced trans-synaptic inputs on the efferent output of the TC neuron. The threshold to drive the efferent output of the neuron at the stimulus frequency decreased with increasing stimulus frequency, and this relationship was unaffected by the presence or absence of trans-synaptic inputs (also see Fig. 8*C*, below). In modeling the stimulation-induced trans-synaptic inputs the goal was not to reproduce a specific type of input to TC relay neurons but to simulate the effect of strong synaptic action generated during DBS as a result of simultaneous activation of large numbers of presynaptic terminals. We conducted a sensitivity analysis by examining the threshold of the TC relay neuron as a function of stimulus frequency after doubling or halving each of the synaptic conductance values (Fig. 6). In general, increasing or decreasing the individual synaptic conductances had limited effects on threshold. Most of the synaptic input parameter sets (including default) were unable to generate action potentials solely from the applied synaptic inputs because of the balance between the excitatory and inhibitory postsynaptic currents. However, in the cases of 2 g_{AMPA} or 0.5 g_{GABAa} the balance was shifted toward excitation and the stimulation-induced trans-synaptic inputs were

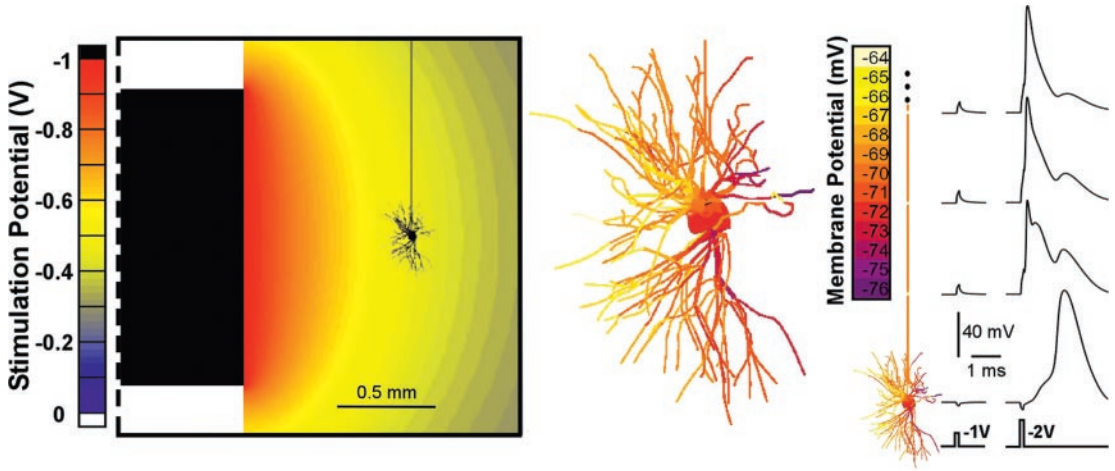

FIG. 4. Action potential initiation occurs in the axon during extracellular stimulation of model thalamocortical (TC) relay neurons. *Left*: neuron model drawn to scale and superimposed on the potential distribution generated by the electrode model. Active electrode contact is black and the dashed line represents the line of axial symmetry. Application of the extracellular potentials to each compartment of the neuron model resulted in the membrane polarization displayed on the right. False color plot of membrane potential displays the neuron polarization induced by a −1 V stimulus, 0.1 ms after onset. Recordings from the soma and nodes of Ranvier show the membrane potential as a function of time for a subthreshold (−1 V) and suprathreshold (−2 V) 0.1 ms stimulus.

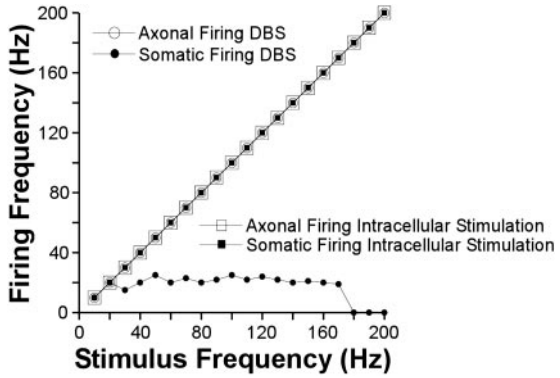

FIG. 5. Intracellular and extracellular high-frequency stimulation generated different firing patterns in the model TC relay neuron. When stimulating intracellularly, suprathreshold (30 nA) 0.1-ms stimuli were applied in the soma. When stimulating extracellularly, the neuron was positioned as in Fig. 4 and activated with −3 V, 0.1 ms stimuli.

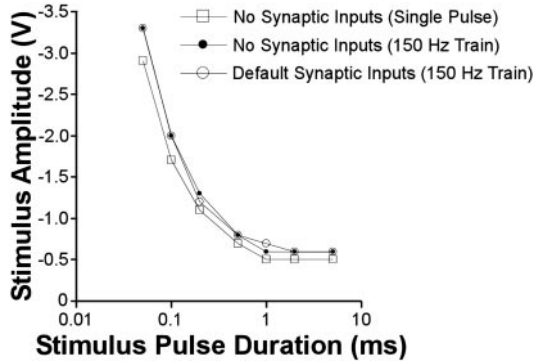

FIG. 7. Strength–duration relationship for extracellular stimulation of the model TC relay neuron positioned as in Fig. 4. Threshold to drive the efferent output of the neuron at the stimulus frequency decreased with increasing stimulus pulse duration.

sufficient to generate efferent output at the stimulus frequency, independent of the applied field. These 2 cases were not plotted in Fig. 6 because the threshold stimulus amplitude was not determined by application of the extracellular electric field to the TC relay neuron, but instead by the activation of axon terminals projecting to the TC relay neuron. Thus with weak GABAa and/or strong AMPA conductances the threshold to drive the efferent output of the TC relay neuron would be determined by the threshold for activation of afferent inputs.

The threshold to activate the TC relay neuron was dependent on the stimulus pulse duration (Fig. 7). We determined the strength–duration (SD) relationship for the TC relay neuron positioned 1.5 mm from the electrode center (as in Fig. 4). The SD relationship can be characterized by rheobase (threshold stimulus amplitude to generate an action potential with infinitely long stimulus pulse) and chronaxie (pulse duration at which threshold stimulus amplitude is 2 × rheobase). We calculated chronaxie using the methods described by Holsheimer et al. (2000a). Driving the TC relay neuron at the stimulus frequency resulted in a chronaxie of 0.21 ms with stimulation-induced trans-synaptic inputs and 0.19 ms without them. These chronaxies were substantially shorter than the single pulse intracellular chronaxie of 6.3 ms, but slightly longer than chronaxies determined for tremor reduction during thalamic DBS (0.05–0.1 ms) (Holsheimer et al. 2000b).

The response of the TC relay neuron was dependent on its position relative to the electrode. Figure 8*A* each neuron was oriented with its axon parallel to the electrode shaft and threshold was calculated to drive the efferent output at 150 Hz using 0.1 ms

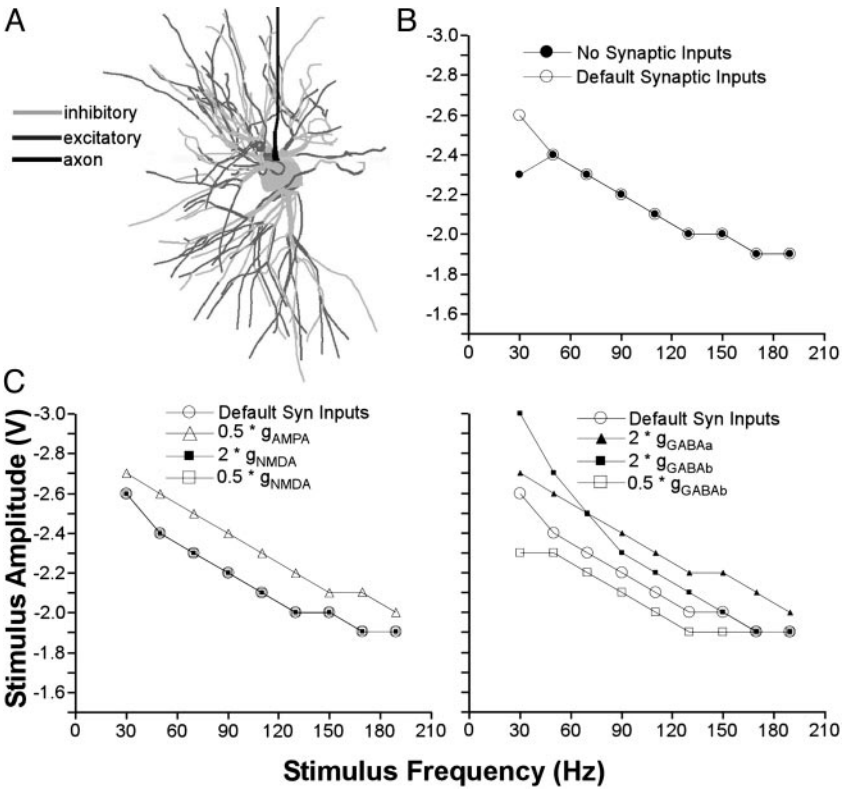

FIG. 6. Stimulation-induced trans-synaptic inputs had a small impact on the excitability of model TC relay neurons. *A*: distribution of somatic and dendritic compartments that received either excitatory or inhibitory synaptic inputs. Plots in *B* and *C* quantify the threshold to drive the efferent output of the neuron, positioned as in Fig. 4, at the stimulus frequency with 0.1 ms extracellular stimulus pulses. *B*: default synaptic inputs had little impact on the stimulation threshold. *C*: sensitivity of the influence of the different types of synapses (AMPA, NMDA, GABAa, GABAb) on excitation threshold were examined by doubling or halving their individual conductance values. In general, altering the synaptic conductances had a slight impact on the excitation thresholds; however, doubling the AMPA conductance or halving the GABAa conductance generated firing at the stimulus frequency resulting solely from the stimulation-induced trans-synaptic inputs and are not plotted.

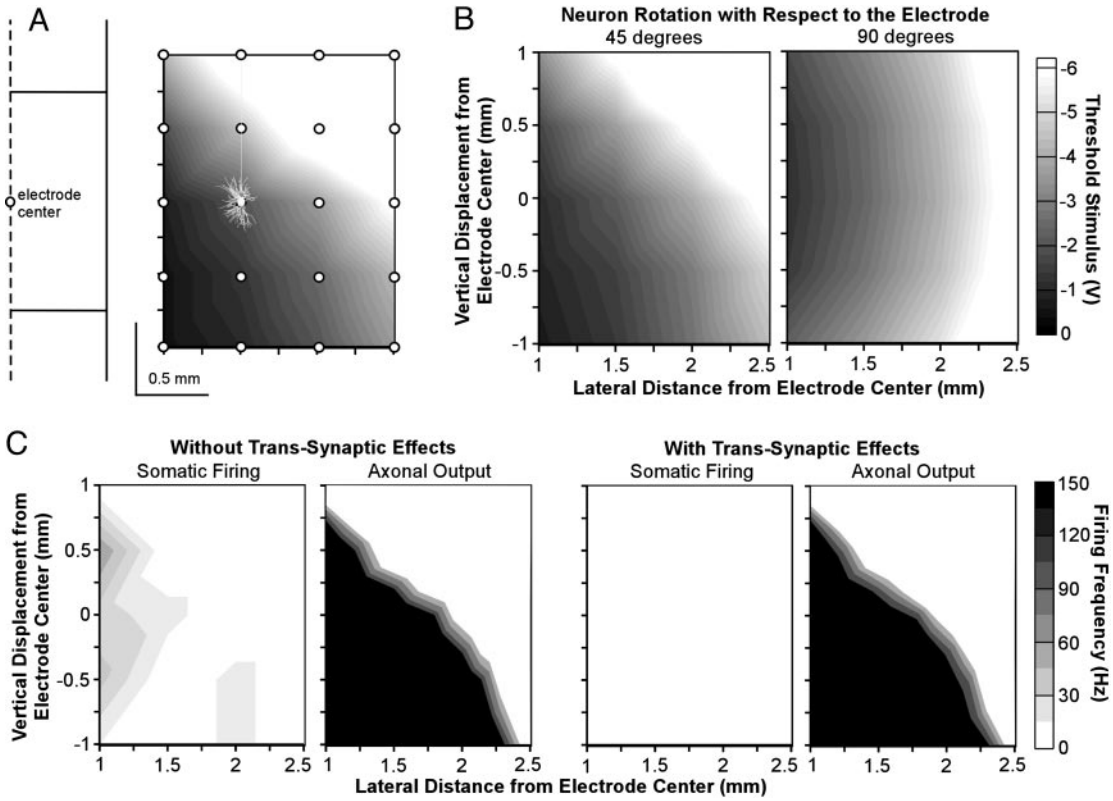

FIG. 8. Influence of neuron position on the effects of extracellular stimulation on model TC relay neurons. *A*: threshold to drive efferent output of the TC relay neuron at 150 Hz using 0.1 ms stimulus pulses as a function of neuron position relative to the electrode. Twenty neurons were oriented with their axons parallel to the electrode shaft and threshold was measured as a function of cell body location (white dots). *B*: neurons from *A* were rotated clockwise 45 and 90° and threshold was calculated. Grayscale threshold values given at right are the same for *A* and *B*. *C*: cell body and axonal firing frequency as a function of cell body location during a −3 V, 0.1 ms, 150 Hz stimulus train. Neurons were oriented as in *A*; however, in regions of sharp transition the neuron spacing interval was reduced to 0.25 mm.

stimulus pulses. This neuron orientation allowed examination of the role of cell body location on threshold with examples of neurons that could also be considered fibers of passage. Each neuron received stimulation-induced trans-synaptic inputs. Neurons positioned in the lower half of Fig. 8*A* had a greater length of their axon passing through the depolarizing influence of the field and as a result had lower thresholds for activation. The axons of the neurons positioned in the upper half of Fig. 8*A* received little or no direct depolarization from the field and in turn required stronger stimulus amplitudes for activation. Activation was also dependent on the axonal orientation with respect to the electrode. Figure 8*B* shows the threshold to drive efferent output at 150 Hz with the neurons rotated 45 and 90° with respect to the electrode axis. The thresholds to excite neurons oriented at 45° were quite similar to those at 0°, whereas larger-stimulus amplitudes were required to excite neurons rotated to 90°. These results were independent of the presence or absence of stimulation-induced trans-synaptic inputs (data not shown).

High-frequency efferent output generated by extracellular stimulation was characterized by limited somatic firing during the stimulus train. Figure 8*C* shows the firing frequency recorded in the cell body and axon as a function of cell body location during a 150-Hz train of −3 V, 0.1 ms stimuli (axons parallel to the electrode shaft). Stimulation with these clinically effective parameters resulted in efferent output at the stimulus frequency in neurons ≤2.25 mm from the electrode but the soma either fired at a much lower frequency or not at all. This decoupling between the firing of the axon and cell body during DBS was independent of the presence or absence of stimulation-induced trans-synaptic inputs (Fig. 8*C*).

Extracellular stimulation of thalamic neurons: effects on firing neurons

The above results were from model neurons stimulated from rest (i.e., there was no activity in the neurons before the stimulus train was applied). However, thalamic neurons are often active in vivo. We examined the effects of DBS on intrinsically active neurons, firing in either a tonic or burst mode. Tonic activity was generated in the TC relay neuron by increasing the Na^+ leakage conductance such that the model generated intrinsic 33-Hz output (Fig. 8). Bursting activity was generated in the TC relay neuron by decreasing the Na^+ leakage conductance, increasing the T-type Ca^{2+} conductance, and shifting the voltage dependency of I_h such that the model generated intrinsic delta oscillations (Figs. 3*D* and 10).

The response of tonically active or bursting TC relay neurons to DBS was nearly identical to that measured in quiescent TC neurons. Figure 9 shows the firing of the cell body and axon of 2 tonically active TC relay neurons before, during, and after a 500-ms train of −3 V, 0.1 ms stimuli at 150 Hz. The stimuli were suprathreshold for activation of the neuron 1.5

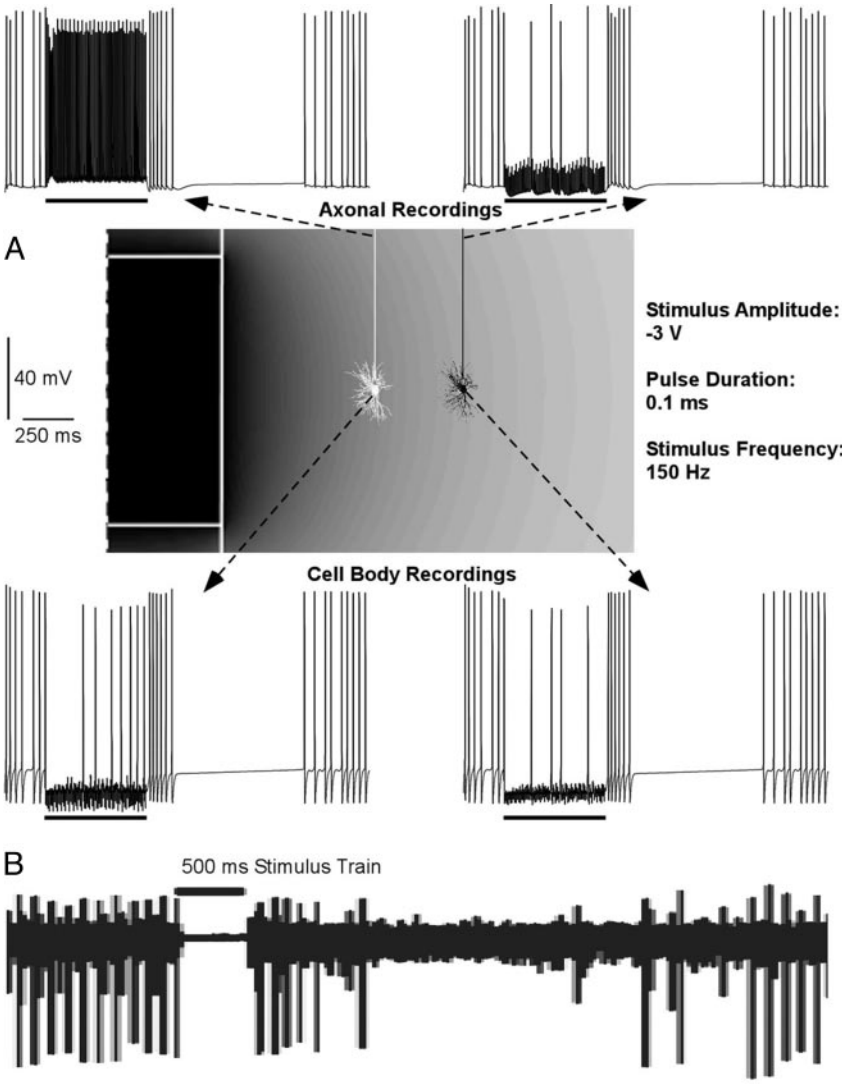

FIG. 9. Effects of DBS on tonically active model TC relay neurons. *A*: recordings from the cell body and axon of 2 tonically active TC relay neurons before, during, and after a 500-ms train of −3 V, 0.1 ms stimuli at 150 Hz (designated with black bars). Stimulus was suprathreshold for direct activation of the white neuron (1.5 mm from the electrode center), but subthreshold for direct activation of the black neuron (2 mm from the electrode center). Both neurons received the default stimulation-induced trans-synaptic inputs during the stimulus train. Neurons were made tonically active (average firing rate = 33 Hz) by increasing the Na^+ leakage conductance (g_{NaL} = 0.0000305 S/cm^2). *B*: human intraoperative recording of a thalamic neuron before and after microstimulation (5 μA, 0.15 ms stimuli at 100 Hz) through the recording electrode (Dostrovsky and Lozano 2002).

mm from the electrode, and generated axonal output in a 1:1 ratio with the stimulus frequency while the intrinsic activity of the cell body was suppressed (Fig. 9*A*). The stimuli were subthreshold for generation of efferent output in the neuron 2 mm from the electrode, and resulted in suppression of the tonic activity during the stimulus train in both the soma and axon as a result of activation of the transsynaptic inputs (Fig. 9*A*). In both cases, the stimulation-induced trans-synaptic inputs generated a cascade of activity patterns after termination of the stimulus train. First there was a rebound of activity, followed by a period of quiescence (~650 ms), followed by a return to 33-Hz firing (Fig. 9*A*).

Recent experimental recordings in humans exhibited responses in thalamic neurons after cessation of short-duration, high-frequency stimulus trains that were quite similar to those of the TC model (Dostrovsky and Lozano 2002; Dostrovsky et al. 2002) (Fig. 9*B*). The origin of the transient quiescence after termination of the stimulation train has not been previously addressed, but our results indicate that it is the result of activation of GABAb receptors. The GABAb conductance was the only component of our model that could generate and/or modulate the transient quiescence in a manner that matched the available experimental data. Decreasing or removing the GABAb conductance decreased or eliminated the transient quiescence in a manner that was dependent on the stimulation frequency and train duration. Similarly, experimental recordings showed that increasing the duration and frequency of the stimulus train enhances the duration of the transient quiescence (Dostrovsky et al. 2002). Therefore our results predict that application of GABAb antagonists would abolish the transient quiescence observed after HFS of thalamic neurons.

Figure 10 shows the activity of the cell body and axon of TC relay neurons firing in a burst mode before, during, and after a 500-ms train of −3-V, 0.1-ms stimuli at 150 Hz. The stimulus was suprathreshold for direct activation of the neuron 1.5 mm from the electrode and its axon fired in a 1:1 ratio with the stimulus train. The soma exhibited a stimulation-induced burst followed by tonic depolarization and a complete suppression of any subsequent burst activity. The stimulus was subthreshold for direct generation of efferent output in the neuron positioned further from the electrode (2 mm), but stimulation-induced trans-synaptic effects still suppressed the delta oscillation. This neuron exhibited a burst at the onset of the stimulus train followed by tonic depolarization and suppression of activity during the stimulus train in both the cell body and axon. The quiescence generated in bursting cells after HFS was the result

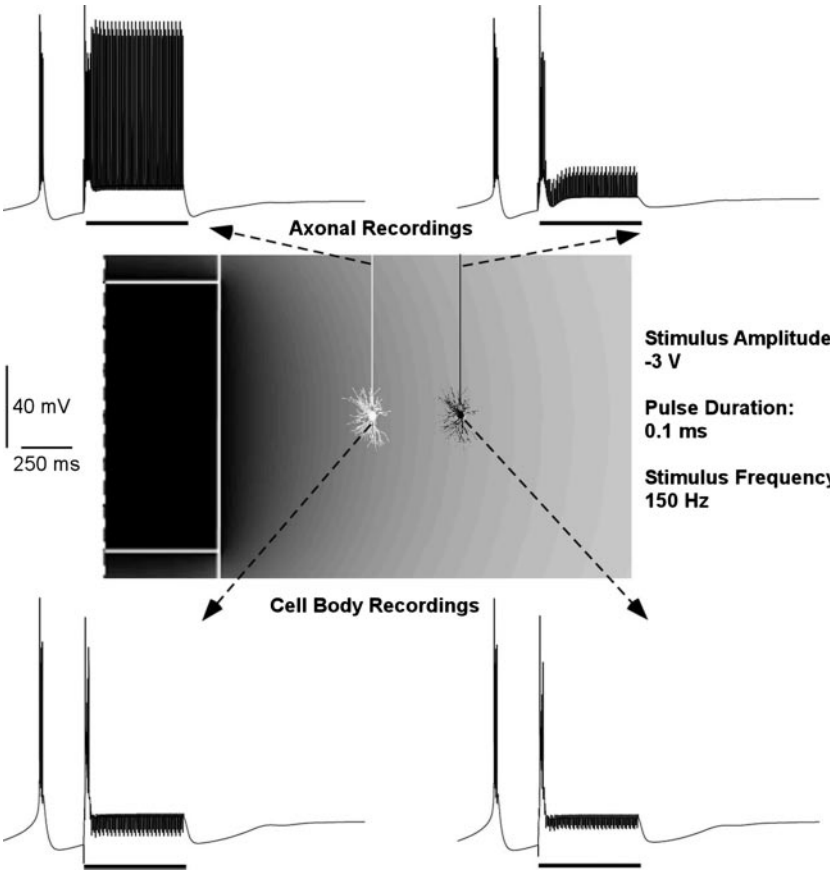

FIG. 10. Effects of DBS on bursting model TC relay neurons. Recordings from the cell body and axon of 2 bursting TC relay neurons before, during, and after a 500 ms train of −3 V, 0.1 ms stimuli at 150 Hz (designated with black bars). Stimulus was suprathreshold for direct activation of the white neuron, but subthreshold for direct activation of the black neuron. Both neurons received the default stimulation-induced trans-synaptic inputs during the stimulus train. Neurons were made to intrinsically burst with the parameter modifications listed in Fig. 3*D*.

of a transition in the operating mode of the cell induced by the stimulation. In dynamical terms, the rhythmic bursting activity of the TC relay neuron was generated by a stable limit cycle determined by the interplay between the hyperpolarization-activated cation current, T-type calcium current, and the potassium leakage current. Application of short-duration trains (10–200 ms) of high-frequency stimuli could disrupt the phase relation of the burst cycle, but did not transform the operating mode of the cell. Application of prolonged stimulus trains (>400 ms) completely disrupted the limit cycle and pushed the neural dynamics into a fixed point or stable resting point. The system would remain in the fixed point until a strong perturbation reintroduced the oscillatory activity.

DISCUSSION

The objective of this study was to develop a quantitative understanding of the effects of DBS on TC relay neurons. Our results support the hypothesis that during HFS the activity in the cell body may be decoupled from activity in the axon, and that a single neuron may simultaneously exhibit suppression of intrinsic activity in the soma and excitation in the axon. Therefore, somatic recordings may yield a different picture of neuronal activity than recordings of axonal output, and this decoupling of activity in the soma and axon during DBS provides a resolution to apparently contradictory experimental results. Two main conclusions can be drawn from this study: *1*) High-frequency DBS generated efferent output at the stimulus frequency in neurons near the electrode. *2*) Stimulation-induced trans-synaptic inputs could suppress intrinsic activity, but had limited effects on the output of neurons whose axon was directly excited by DBS.

Model limitations

The results obtained with our model of thalamic DBS provide insights difficult to achieve experimentally; however, both the electrode and neuron models have important limitations that should be noted. One limitation of our electrode model is that we assumed the tissue medium was isotropic. Although this may be a valid approximation within the thalamus, the anatomical structures surrounding the thalamus, such as the internal capsule, are highly anisotropic. The anisotropic nature of the tissue surrounding the stimulated nucleus can affect the shape of the electric field and in turn neural polarization (Grill 1999). However, our previous experience with stimulation in a gray matter region surrounded by white matter fiber tracks suggests that the influence of the anisotropy is a secondary concern (McIntyre and Grill 2002).

The multi-compartment TC relay neuron model accurately captured dynamic firing properties recorded experimentally, but limitations in the model arise from our limited knowledge of the ion channel distribution of the TC relay neuron dendritic arbor (Antal et al. 2001; Emri et al. 2000; Williams and Stuart 2000). However, the results of this and previous work addressing the biophysics of extracellular stimulation of CNS neurons suggest that the neural output that results from the stimulation is primarily dependent on the myelinated axon of the neuron (McIntyre and Grill 1999; Rattay 1999). The myelinated axon model used in this study consisted of a detailed representation

of the fiber morphology and ion channel distribution and was able to capture nearly every experimentally recorded firing property of myelinated axons (McIntyre et al. 2002).

Another limitation of our model was the lack of inclusion of activity-dependent changes in synaptic efficacy such as short- and long-term potentiation and/or depression. In addition, the afferent axons and terminals presynaptic to the TC relay neuron were not explicitly defined in the model. We acknowledge that these limitations in our stimulation-induced trans-synaptic inputs could play important roles in determining the trans-synaptic effects of DBS. However, our sensitivity analysis of the role of individual synaptic conductances on neural output shows that doubling or halving the conductances resulted in $<10\%$ changes in threshold as a function of stimulus frequency (Fig. 6). Moreover, inclusion of trans-synaptic effects in our model did not strongly influence any of the results of this study (Figs. 6–8). Therefore we expect activity-dependent changes in the efficacy of synaptic inputs to have a minimal impact on the effects of thalamic DBS on TC relay neurons. However, activity-dependent changes in synaptic efficacy could have important consequences on the downstream effects mediated by high-frequency activation of efferent axons (Urbano et al. 2002; Wang and Kaczmarek 1998; Zucker and Regehr 2002).

Our model also ignored K^+ accumulation in the extracellular space surrounding the neural structure. When neurons fire at high frequencies for extended periods of time they (and/or the surrounding glia) can release large amounts of K^+ into the extracellular space, resulting in changes in osmolarity and excitability (Bikson et al. 2001; Lian et al. 2003). Increases in the extracellular K^+ concentration ($[K^+]_o$) can result in depolarization block where the membrane becomes so depolarized that Na^+ channels become inactivated (Hille 2001). The magnitude and time course of the changes in $[K^+]_o$ that occur during DBS are presently unknown, and we did not attempt to model these phenomena. Therefore because of the lack of inclusion of activity-dependent changes in synaptic efficacy and K^+ accumulation in the extracellular space our model is unable to predict accurately the long-term effects of DBS.

Activation and suppression of neuronal activity by DBS

Our results predict that thalamic DBS results in regions of both activation and suppression of efferent output. These results match well with experimental recordings from both the stimulated nucleus and nuclei receiving the efferent output during DBS. Single-unit recordings in the thalamus and basal ganglia consistently reveal a suppression of activity within the stimulated nucleus during HFS (Boraud et al. 1996; Dostrovsky and Lozano 2002; Dostrovsky et al. 2000). However, activity recorded in projection nuclei suggests that there is increased input from the stimulated nucleus during HFS (Anderson et al. 2003; Hashimoto et al. 2003; Maurice et al. 2003; Windels et al. 2000, 2003). These experimental results seem to be contradictory, although the results of our study match both of these findings. Recordings from the cell body of our model showed suppression of activity during HFS, but activity recorded in the cell body was not representative of the neural output generated in the axon (Figs. 8–10). Our results predict that the majority of neurons within about 2 mm of the electrode contact will generate efferent output at the stimulus frequency, providing high-frequency inputs to projection nuclei, even though activity in the somas of these neurons is suppressed.

Two fundamental effects of extracellular stimulation support the finding of decoupling of activity in the axon and cell body during HFS: *1*) action potential initiation in the axon and *2*) stimulation-induced trans-synaptic inputs. The direct effect of an applied electric field on a neuron is related to the second derivative of the extracellular potential distribution along each process (McNeal 1976; Rattay 1986). In turn, each neuron (or neural process) surrounding the electrode will be subject to both depolarizing and hyperpolarizing effects from the stimulation (McIntyre and Grill 1999; Rattay 1999) (Fig. 4). In general, cathodic stimuli generate membrane depolarization in regions near the electrode and membrane hyperpolarization in regions that flank the region of depolarization. However, because of the 3-D branching and termination patterns of the dendritic arbor, soma–dendritic complexes near the electrode exhibit both depolarization and hyperpolarization. The applied field generates depolarization in dendritic processes that terminate closer to the electrode and hyperpolarization in dendritic processes that terminate further from the electrode (Fig. 4). Depending on the neuron's orientation and positioning with respect to the electrode, it is common for the cell body to be directly hyperpolarized by the stimulus pulse. However, the first few nodes of Ranvier are usually depolarized by the stimulus pulse because of the short internodal spacing of the axon compared with the spatial distribution of potentials generated by the macroelectrode (Fig. 4). In turn, action potential initiation occurs in the axon (McIntyre and Grill 1999, 2002; Nowak and Bullier 1998a,b).

The second effect of extracellular stimulation that supports the decoupling of activity in the axon and cell body during HFS is the activation of trans-synaptic inputs. The threshold for extracellular stimulation of axonal terminals projecting to the region around the electrode is lower than the threshold for direct activation of local cells (Baldissera et al. 1972; Dostrovsky et al. 2000; Gustafsson and Jankowska 1976; Jankowska et al. 1975). The stimulation-induced trans-synaptic effects generated in postsynaptic neurons by the stimulation can affect their response to trains of extracellular stimuli. The relative distribution of excitatory and inhibitory synaptic inputs on the soma–dendritic membrane of TC relay neurons (and neurons in general) provides for a concentration of inhibitory inputs on the soma and proximal dendrites (Sato et al. 1997) (Fig. 6). Summation of an overall inhibitory synaptic effect on the cell body during high-frequency extracellular stimulation can aid in the generation of independent firing of the axon and cell body (Fig. 8).

Trans-synaptic effects applied to TC relay neurons subthreshold for direct excitation by DBS did reduce the activity of intrinsically active model neurons (Figs. 9 and 10). However, synaptic inputs did not dramatically alter the output of neurons during DBS with stimuli suprathreshold for direct excitation (Figs. 6–8). This result was robust to large changes in the synaptic conductance values (Fig. 6) because action potential initiation always occurred in the axon (Fig. 4). The change in excitability of the cell body and dendrites from the synaptic inputs had limited impact on the axon and, as a result, the output from suprathreshold stimuli was relatively unaffected by the synaptic influences.

Implications for understanding the therapeutic mechanisms of DBS

Presently, there are 4 general hypotheses to explain the therapeutic mechanism(s) of DBS: *1*) stimulation-induced alterations in voltage-gated currents that block neural output near the stimulating electrode (Depolarization Blockade) (Beurrier et al. 2001); *2*) stimulation-induced trans-synaptic inhibition of neurons near the stimulating electrode (Synaptic Inhibition) (Dostrovsky et al. 2000); *3*) synaptic transmission failure of the efferent output of stimulated neurons as a result of transmitter depletion (Synaptic Depression) (Urbano et al. 2002); *4*) stimulation-induced modulation of pathological network activity (Hashimoto et al. 2003; Montgomery and Baker 2000).

Depolarization blockade and synaptic inhibition represent two of the earliest hypotheses to explain the similarity between the therapeutic benefit of ablation and DBS for the treatment of movement disorders. Both of these effects are supported by recordings of somatic activity in the stimulated nucleus from several different types of experimental preparations (in vitro and in vivo, humans and animals) (Benazzouz et al. 1995, 2000; Beurrier et al. 2001; Bikson et al. 2001; Boraud et al. 1996; Dostrovsky et al. 2000; Kiss et al. 2002; Lian et al. 2003). However, our results suggest the limitation of these hypotheses is that they do not take into account the possible independent activation of the efferent axon. The axon plays a critical role in the activation of neurons by extracellular stimulation, and the response of the cell body does not necessarily reflect the output of the axon (Figs. 8–10). Therefore although synaptic inhibition and/or depolarization blockade may occur in the cell body, the suppression of somatic activity will have limited impact on the output of neurons whose axons are directly excited by DBS.

How then can stimulation that results in efferent output of neurons around the electrode mimic the therapeutic effects of ablation? One possibility is that neurons activated by the stimulus train are unable to sustain high-frequency action on efferent targets because of depletion of neurotransmitter (Urbano et al. 2002; Wang and Kaczmarek 1998; Zucker and Regehr 2002). However, several in vivo experimental studies have shown increases in transmitter release and sustained changes in firing of neurons in efferent nuclei consistent with activation of neurons around the electrode and subsequent synaptic action on their target during HFS (Anderson et al. 2003; Hashimoto et al. 2003; Windels et al. 2000, 2003). Therefore the only general hypothesis on the mechanisms of DBS that is consistent with all of the available data on the effects of DBS (including the results of this study) is stimulation-induced modulation of pathological network activity. However, it should be noted that, although DBS may override pathological activity patterns, the activity patterns induced by DBS are not normal. Therefore it remains an open question to link the cellular effects of DBS with explicit therapeutic mechanisms.

The control of tremor with DBS may be explained by blocking low-frequency oscillations. Tremor is most likely generated by increased neuronal synchronization and low-frequency rhythmic oscillation within the basal ganglia and thalamus (Bergman et al. 1998; Deuschl et al. 2001). Our results suggest that DBS masks the underlying activity of neurons surrounding the electrode, independent of their original mode of operation: rest (Figs. 6, 7, 9), tonically active (Fig. 9), or bursting (Fig. 10). This masking can result from either stimulation-induced trans-synaptic suppression of activity or efferent firing time-locked to the stimulus frequency. In either case the firing patterns of neurons directly affected by DBS are no longer regulated by their network interactions, but instead by the constant and unchanging stimulation. Therefore we propose that, independent of their response to DBS, neurons directly affected by DBS represent a barrier for the transmission of synchronized low-frequency oscillations throughout the network.

APPENDIX

The ionic currents of the neural models can be written in the general form of

$$I_{ion} = g_{ion}(V_m - E_{ion})$$

where g_{ion} is the maximum conductance for the individual ion channel (Tables 2 and 3) multiplied by gating variables that range from 0 to 1. The time and voltage dependency of each gating parameter (ω) is given by

$$\tau_\omega = 1/(\alpha_\omega + \beta_\omega)$$

$$d\omega/dt = \alpha_\omega(1 - \omega) - \beta_\omega\omega = (\omega_\infty - \omega)/\tau_\omega$$

where the time course and magnitude of the activation and inactivation parameters used in the simulations are given below. The membrane dynamics were based on the experimental references given in METHODS and the previous modeling work of Destexhe et al. (1998) and Huguenard and McCormick (1992). The models were implemented in NEURON v5.3 (Hines and Carnevale 1997) using a time step of 0.01 ms and a temperature of 36°C. Individuals interested in reproducing the results of this study or using these models in their own work are encouraged to contact us for the appropriate NEURON files and instruction on their use. Times are in ms, voltages are in mV, concentrations are in mM, and currents are in mA/cm^2.

Soma and dendrite T-type Ca^+ current

$$I_{CaT} = P_{CaT}m^2hG(V_m, Ca_o, Ca_i)$$

$$G(V_m, Ca_o, Ca_i) = Z^2F^2V_m/RT \times [(Ca_i - Ca_oe^{\{-ZFV_m/RT\}})/1 - e^{\{-ZFV_m/RT\}}]$$

$$Ca_o = 2; \quad Ca_i(t = 0) = 0.00024$$

$$dCa_i/dt = [(0.00024 - Ca_i)/5] - [I_{CaT}/(ZF \times 10^{-5})]$$

$$\tau_m = 0.333/[e^{\{-(V_m+135)/16.7\}} + e^{\{(V_m+19.8)/18.2\}}] + 0.204$$

$$m_\infty = 1/[1 + e^{\{-(V_m+60)/6.2\}}]$$

$$V_m < -80, \quad \tau_h = 0.333e^{\{(V_m+470)/66.6\}};$$

$$V_m > -80, \quad \tau_h = 9.33 + 0.333e^{\{-(V_m+25)/10.5\}}$$

$$h_\infty = 1/[1 + e^{\{(V_m+84)/4\}}]$$

Soma and dendrite hyperpolarization activated cation current

$$I_h = g_hm^3(V_m + 43)$$

$$\tau_m = 1/[e^{\{-15.45-(0.086V_m)\}} + e^{\{-1.17+(0.0701V_m)\}}]$$

$$m_\infty = 1/[e^{\{(V_m+85)/5.5\}} + 1]$$

Soma, dendrite, and initial-segment fast Na^+ current

$$I_{Naf} = g_{Naf} m^3 h (V_m - E_{Na})$$

$$\alpha_m = [0.32(-(V_m + 55))]/[e^{\{-(V_m+55)/4\}} - 1]$$

$$\beta_m = [0.28(V_m + 28)]/[e^{\{(V_m+28)/5\}} - 1]$$

$$\alpha_h = 0.128e^{\{-(V_m+51)/18\}}$$

$$\beta_h = 4/[e^{\{-(V_m+28)/5\}} + 1]$$

Soma, dendrite, and initial-segment delayed rectifier K^+ current

$$I_{Kdr} = g_{Kdr} m^4 (V_m - E_K)$$

$$\alpha_m = [0.032(-(V_m + 63.8))]/[e^{\{-(V_m+63.8)/5\}} - 1]$$

$$\beta_m = 0.5e^{\{-(V_m+68.8)/40\}}$$

Soma, dendrite, and initial-segment slow K^+ current

$$I_{Ks} = g_{Ks} m((0.4h1) + (0.6h2))(V_m - E_K)$$

$$\tau_m = 0.253/[e^{\{(V_m-81)/25.6\}} + e^{\{(V_m+132)/-18\}}] + 2.5$$

$$m_\infty = (1/[1 + e^{\{-(V_m+43)/17\}}])^4$$

$$\tau_{h1} = 0.253/[e^{\{(V_m-1329)/200\}} + e^{\{-(V_m+130)/7.1\}}] + 30.4$$

$$h1_\infty = h2_\infty = 1/[1 + e^{\{(V_m+58)/10.6\}}]$$

$$V_m < -70, \quad \tau_{h2} = \tau_{h1}; \quad V_m > -70, \quad \tau_{h2} = 2{,}260$$

Nodal fast Na^+ current

$$I_{Naf} = g_{Naf} m^3 h (V_m - E_{Na})$$

$$\alpha_m = [6.57(V_m + 11.4)]/[1 - e^{\{-(V_m+11.4)/10.3\}}]$$

$$\beta_m = [0.304(-(V_m + 15.7))]/[1 - e^{\{(V_m+15.7)/9.16\}}]$$

$$\alpha_h = [0.34(-(V_m + 104))]/[1 - e^{\{(V_m+104)/11\}}]$$

$$\beta_h = 12.6/[1 + e^{\{-(V_m+21.8)/13.4\}}]$$

Nodal persistent Na^+ current

$$I_{Nap} = g_{Nap} p^3 (V_m - E_{Na})$$

$$\alpha_p = [0.0353(V_m + 17)]/[1 - e^{\{-(V_m+17)/10.2\}}]$$

$$\beta_p = [0.000883(-(V_m + 24))]/[1 - e^{\{(V_m+24)/10\}}]$$

Nodal slow K^+ current

$$I_{Ks} = g_{Ks} s (V_m - E_K)$$

$$\alpha_s = 0.3/[1 + e^{\{(V_m+43)/-5\}}]$$

$$\beta_s = 0.03/[1 + e^{\{(V_m+80)/-1\}}]$$

Juxtaparanodal (FLUT) fast K^+ current

$$I_{Kf} = g_{Kf} n^4 (V_m - E_K)$$

$$\alpha_n = [0.0462(V_m + 83.2)]/[1 - e^{\{-(V_m+83.2)/1.1\}}]$$

$$\beta_n = [0.0824(-(V_m + 66))]/[1 - e^{\{(V_m+66)/10.5\}}]$$

ACKNOWLEDGMENTS

We thank Dr. Alain Destexhe for providing the 3-D reconstruction of the thalamocortical relay neuron.

GRANTS

This work was supported by National Institute of Neurological Disorders and Stroke Grants NS-40894 and NS-35528 and a postdoctoral fellowship supported by the Whitaker Foundation.

REFERENCES

Anderson ME, Postupna N, and Ruffo M. Effects of high-frequency stimulation in the internal globus pallidus on the activity of thalamic neurons in the awake monkey. *J Neurophysiol* 89: 1150–1160, 2003.

Antal K, Emri Z, and Crunelli V. On the invasion of distal dendrites of thalamocortical neurones by action potentials and sensory EPSPs. *Thalamus Rel Syst* 1: 105–116, 2001.

Baldissera F, Lundberg A, and Udo M. Stimulation of pre- and postsynaptic elements in the red nucleus. *Exp Brain Res* 15: 151–167, 1972.

Benabid AL, Koudsie A, Pollak P, Kahane P, Chabardes S, Hirsch E, Marescaux C, and Benazzouz A. Future prospects of brain stimulation. *Neurol Res* 22: 237–246, 2000.

Benabid AL, Pollak P, Gao D, Hoffmann D, Limousin P, Gay E, Payen I, and Benazzouz A. Chronic electrical stimulation of the ventralis intermedius nucleus of the thalamus as a treatment of movement disorders. *J Neurosurg* 84: 203–214, 1996.

Benazzouz A, Gao DM, Ni ZG, Piallat B, Bouali-Benazzouz R, and Benabid AL. Effect of high-frequency stimulation of the subthalamic nucleus on the neuronal activities of the substantia nigra pars reticulata and ventrolateral nucleus of the thalamus in the rat. *Neuroscience* 99: 289–295, 2000.

Benazzouz A, Piallat B, Pollak P, and Benabid AL. Responses of substantia nigra pars reticulata and globus pallidus complex to high frequency stimulation of the subthalamic nucleus in rats: electrophysiological data. *Neurosci Lett* 189: 77–80, 1995.

Bergman H, Feingold A, Nini A, Raz A, Slovin H, Abeles M, and Vaadia E. Physiological aspects of information processing in the basal ganglia of normal and parkinsonian primates. *Trends Neurosci* 21: 32–38, 1998.

Beurrier C, Bioulac B, Audin J, and Hammond C. High-frequency stimulation produces a transient blockade of voltage-gated currents in subthalamic neurons. *J Neurophysiol* 85: 1351–1356, 2001.

Bikson M, Lian J, Hahn PJ, Stacey WC, Sciortino C, and Durand DM. Suppression of epileptiform activity by high frequency sinusoidal fields in rat hippocampal slices. *J Physiol* 531: 181–191, 2001.

Boraud T, Bezard E, Bioulac B, and Gross C. High frequency stimulation of the internal globus pallidus (GPi) simultaneously improves parkinsonian symptoms and reduces the firing frequency of GPi neurons in the MPTP-treated monkey. *Neurosci Lett* 215: 17–20, 1996.

Destexhe A, Mainen ZF, and Sejnowski TJ. An efficient method for computing synaptic conductances based on a kinetic model of receptor binding. *Neural Comput* 6: 14–18, 1994a.

Destexhe A, Mainen ZF, and Sejnowski TJ. Synthesis of models for excitable membranes, synaptic transmission and neuromodulation using a common kinetic formalism. *J Comput Neurosci* 1: 195–230, 1994b.

Destexhe A, Neubig M, Ulrich D, and Huguenard J. Dendritic low-threshold calcium currents in thalamic relay cells. *J Neurosci* 18: 3574–3588, 1998.

Deuschl G, Raethjen J, Lindemann M, and Krack P. The pathophysiology of tremor. *Muscle Nerve* 24: 716–735, 2001.

Dostrovsky JO, Levy R, Wu JP, Hutchison WD, Tasker RR, and Lozano AM. Microstimulation-induced inhibition of neuronal firing in human globus pallidus. *J Neurophysiol* 84: 570–574, 2000.

Dostrovsky JO and Lozano AM. Mechanisms of deep brain stimulation. *Mov Disord* 17(Suppl 3): 63–68, 2002.

Dostrovsky JO, Patra S, Hutchison WD, Palter VN, Filali M, and Lozano AM. Effects of stimulation in human thalamus on activity of nearby thalamic neurons. *Soc Neurosci Abstr* 62.14, 2002.

Emri Z, Antal K, Toth TI, Cope DW, and Crunelli V. Backpropagation of the delta oscillation and the retinal excitatory postsynaptic potential in a multi-compartment model of thalamocortical neurons. *Neuroscience* 98: 111–127, 2000.

Greenberg RJ, Velte TJ, Humayun MS, Scarlatis GN, and de Juan E Jr. A computational model of electrical stimulation of the retinal ganglion cell. *IEEE Trans Biomed Eng* 46: 505–514, 1999.

Grill WM. Modeling the effects of electric fields on nerve fibers: influence of tissue electrical properties. *IEEE Trans Biomed Eng* 46: 918–928, 1999.

Grill WM and McIntyre CC. Extracellular excitation of central neurons: implications for the mechanisms of deep brain stimulation. *Thalamus Rel Syst* 1: 269–277, 2001.

Gross RE and Lozano AM. Advances in neurostimulation for movement disorders. *Neurol Res* 22: 247–258, 2000.

Gustafsson B and Jankowska E. Direct and indirect activation of nerve cells by electrical pulses applied extracellularly. *J Physiol* 258: 33–61, 1976.

Hashimoto T, Elder CM, Okun MS, Patrick SK, and Vitek JL. Stimulation of the subthalamic nucleus changes the firing pattern of pallidal neurons. *J Neurosci* 23: 1916–1923, 2003.

Hille B. *Ionic Channels of Excitable Membranes*. Sunderland, MA: Sinauer, 2001.

Hines ML and Carnevale NT. The NEURON simulation environment. *Neural Comput* 9: 1179–209, 1997.

Holsheimer J, Demeulemeester H, Nuttin B, and de Sutter P. Identification of the target neuronal elements in electrical deep brain stimulation. *Eur J Neurosci* 12: 4573–4577, 2000b.

Holsheimer J, Dijkstra EA, Demeulemeester H, and Nuttin B. Chronaxie calculated from current-duration and voltage-duration data. *J Neurosci Methods* 97: 45–50, 2000a.

Huguenard JR and McCormick DA. Simulation of the currents involved in rhythmic oscillations in thalamic relay neurons. *J Neurophysiol* 68: 1373–1383, 1992.

Jahnsen H and Llinas R. Electrophysiological properties of guinea-pig thalamic neurones: an in vitro study. *J Physiol* 349: 205–226, 1984.

Jankowska E, Padel Y, and Tanaka R. The mode of activation of pyramidal tract cells by intracortical stimuli. *J Physiol* 249: 617–636, 1975.

Kiss ZH, Mooney DM, Renaud L, and Hu B. Neuronal response to local electrical stimulation in rat thalamus: physiological implications for mechanisms of deep brain stimulation. *Neuroscience* 113: 137–143, 2002.

Lee DC and Grill WM. Polarization of spherical cells by non-uniform electric fields: steady-state analysis. *Ann Biomed Eng* 29: S128, 2001.

Lian J, Bikson M, Sciortino C, Stacey WC, and Durand DM. Local suppression of epileptiform activity by electrical stimulation in rat hippocampus in vitro. *J Physiol* 547: 427–434, 2003.

Maurice N, Thierry AM, Glowinski J, and Deniau JM. Spontaneous and evoked activity of substantia nigra pars reticulata neurons during high-frequency stimulation of the subthalamic nucleus. *J Neurosci* 23: 9929–9936, 2003.

McCormick DA and Huguenard JR. A model of the electrophysiological properties of thalamocortical relay neurons. *J Neurophysiol* 68: 1384–1400, 1992.

McIntyre CC and Grill WM. Excitation of central nervous system neurons by nonuniform electric fields. *Biophys J* 76: 878–888, 1999.

McIntyre CC and Grill WM. Finite element analysis of the current-density and electric field generated by metal microelectrodes. *Ann Biomed Eng* 29: 227–235, 2001.

McIntyre CC and Grill WM. Extracellular stimulation of central neurons: influence of stimulus waveform and frequency on neuronal output. *J Neurophysiol* 88: 1592–1604, 2002.

McIntyre CC, Richardson AG, and Grill WM. Modeling the excitability of mammalian nerve fibers: influence of afterpotentials on the recovery cycle. *J Neurophysiol* 87: 995–1006, 2002.

McIntyre CC and Thakor NV. Uncovering the mechanisms of deep brain stimulation for Parkinson's disease through functional imaging, neural recording, and neural modeling. *Crit Rev Biomed Eng* 30: 249–281, 2002.

McNeal DR. Analysis of a model for excitation of myelinated nerve. *IEEE Trans Biomed Eng* 23: 329–337, 1976.

Montgomery EB and Baker KB. Mechanisms of deep brain stimulation and future technical developments. *Neurol Res* 22: 259–266, 2000.

Nowak LG and Bullier J. Axons, but not cell bodies, are activated by electrical stimulation in cortical gray matter. I. Evidence from chronaxie measurements. *Exp Brain Res* 118: 477–488, 1998a.

Nowak LG and Bullier J. Axons, but not cell bodies, are activated by electrical stimulation in cortical gray matter. II. Evidence from selective inactivation of cell bodies and axon initial segments. *Exp Brain Res* 118: 489–500, 1998b.

Obeso JA, Olanow CW, Rodriguez-Oroz MC, Krack P, Kumar R, and Lang AE. Deep-brain stimulation of the subthalamic nucleus or the pars interna of the globus pallidus in Parkinson's disease. *N Engl J Med* 345: 956–963, 2001.

O'Suilleabhain PE, Frawley W, Giller C, and Dewey RB Jr. Tremor response to polarity, voltage, pulsewidth and frequency of thalamic stimulation. *Neurology* 60: 786–790, 2003.

Pape HC and McCormick DA. Electrophysiological and pharmacological properties of interneurons in the cat dorsal lateral geniculate nucleus. *Neuroscience* 68: 1105–1125, 1995.

Plonsey R and Heppner DB. Considerations of quasi-stationarity in electrophysiological systems. *Bull Math Biophys* 29: 657–664, 1967.

Rattay F. Analysis of models for external stimulation of axons. *IEEE Trans Biomed Eng* 33: 974–977, 1986.

Rattay F. The basic mechanism for the electrical stimulation of the nervous system. *Neuroscience* 89: 335–346, 1999.

Sances A and Larson SJ. Impedance and current density studies. In: *Electroanesthesia: Biomedical and Biophysical Studies*, edited by Sances A and Larson SJ. New York: Academic Press, 1975, p. 114–124.

Sato F, Nakamura Y, and Shinoda Y. Serial electron microscopic reconstruction of axon terminals on physiologically identified thalamocortical neurons in the cat ventral lateral nucleus. *J Comp Neurol* 388: 613–631, 1997.

Schlag J and Villablanca J. A quantitative study of temporal and spatial response patterns in a thalamic cell population electrically stimulated. *Brain Res* 8: 255–270, 1968.

Urbano FJ, Leznik E, and Llinas RR. Cortical activation patterns evoked by afferent axons stimuli at different frequencies: an in vitro voltage-sensitive dye imaging study. *Thalamus Rel Syst* 1: 371–378, 2002.

Vitek JL. Mechanisms of deep brain stimulation: excitation or inhibition. *Mov Disord* 17(Suppl 3): 69–72, 2002.

Volkmann J, Herzog J, Kopper F, and Deuschl G. Introduction to the programming of deep brain stimulators. *Mov Disord* 17(Suppl 3): 181–187, 2002.

Wang LY and Kaczmarek LK. High-frequency firing helps replenish the readily releasable pool of synaptic vesicles. *Nature* 394: 384–388, 1998.

Williams SR and Stuart GJ. Action potential backpropagation and somatodendritic distribution of ion channels in thalamocortical neurons. *J Neurosci* 20: 1307–1317, 2000.

Windels F, Bruet N, Poupard A, Feuerstein C, Bertrand A, and Savasta M. Influence of the frequency parameter on extracellular glutamate and gamma-aminobutyric acid in substantia nigra and globus pallidus during electrical stimulation of subthalamic nucleus in rats. *J Neurosci Res* 72: 259–267, 2003.

Windels F, Bruet N, Poupard A, Urbain N, Chouvet G, Feuerstein C, and Savasta M. Effects of high frequency stimulation of subthalamic nucleus on extracellular glutamate and GABA in substantia nigra and globus pallidus in the normal rat. *Eur J Neurosci* 12: 4141–4146, 2000.

Zucker RS and Regehr WG. Short-term synaptic plasticity. *Annu Rev Physiol* 64: 355–405, 2002.